Electronic Supplementary Information

Computation Assisted Design of Favored Composition for Ternary Mg-Cu-Y Metallic Glass Formation

Q. Wang, J. H. Li, and B. X. Liu*

Key Laboratory of Advanced Materials (MOE), School of Materials Science and Engineering

Tsinghua University, Beijing 100084, CHINA

Corresponding author e-mail address: dmslbx@tsinghua.edu.cn

1. Smoothed and Long-range TB-SMA Potential

Based on the concept of local electron density, significant progress in realistic potentials has been made during the 1980s by developing the so-called many-body, or *n*-body potentials, such as second-moment approximation of tight-binding (TB-SMA) potential,[1-3] Finnis-Sinclair (FS) potential,[4] embedded-atom method (EAM) potential and their various modifications.[5-7] By rule of thumb, these various *n*-body potentials are suitable for systems of different characteristics. For example, it has been shown that the EAM and F-S potentials are applicable to *fcc* and *bcc* metals, while the TB-SMA potential is more suitable for *fcc* and *hcp* metals.

The TB-SMA potential was first proposed by Tomanek and Rosato.[1] According to the TB-SMA scheme, the energy of the *d* band is proportional to the square root of the second moment of the density of states, while the latter is expressed by a sum of the squares of the hopping/transfer integrals.[1] Accordingly, the total potential energy

of an atom *i* can be written as

$$E_i = \sum_{j \neq i} \phi(r_{ij}) - \sqrt{\sum_j f^2(r_{ij})} \tag{1}$$

where $\phi(r_{ij})$ is the repulsive interaction, and $f(r_{ij})$ is the hopping integrals between atoms *i* and *j* separated by distance r_{ij}. In the TB-SMA scheme proposed by Rosato and Cleri *et al*.,[2,3] the $\phi(r_{ij})$ and $f(r_{ij})$ are taken to be exponential forms:

$$\phi(r_{ij}) = A \exp[-p(\frac{r_{ij}}{r_0} - 1)] \tag{2}$$

$$f(r_{ij}) = \xi^2 \exp[-2q(\frac{r_{ij}}{r_0} - 1)] \tag{3}$$

where r_0 is the first neighboring distance, p, q, A and ξ are four adjustable parameters. From a physical viewpoint, q describes the distance dependence of the hopping/transfer integrals.

For simplifying programming as well as saving computer resources, a cutoff radius is frequently established, and when the distance is greater than the cutoff radius, the interaction between atoms is disregarded. However, some problems may arise in the practical application of the cutoff radius. For example, the summations in Eq. (1) are restricted to the first neighbors in the study of Rosato *et al*.[3] Unfortunately, the potential is not equal to zero at the cutoff radius, thus this treatment creates a problem, *i.e.* whenever an atom-pair 'crosses' the cutoff radius, the energy makes a little 'jump'. A large number of these events could spoil the energy conservation or lead to some non-physical behaviors in the simulations.[8] Besides, the atomic configurations in the first and second neighbors of *fcc* and *hcp* structures are quite similar, and as a result, the energy difference between them is considerably small and cannot be well

distinguished by the short-range potentials with a relatively small cutoff radius.

To solve these problems, the authors' group has proposed a revised formulism, *i.e.*, the formulism of the smoothed and long-range TB-SMA,[9,10] by incorporating a binomial truncation function in the original TB-SMA potential. The expression of the smoothed and long-range TB-SMA potential can be written as follows:

$$E_i = \sum_{j \neq i} \phi(r_{ij}) - \sqrt{\sum_{j \neq i} \psi(r_{ij})} \tag{4}$$

$$\phi(r_{ij}) = \begin{cases} A_1 \exp[-p_1(\frac{r_{ij}}{r_0} - 1)], & r_{ij} \leq r_{m1} \\ A_{1m} \exp[-p_{1m}(\frac{r_{ij}}{r_0} - 1)](\frac{r_{c1}}{r_0} - \frac{r_{ij}}{r_0})^{n1}, & r_{m1} < r_{ij} \leq r_{c1} \end{cases} \tag{5}$$

$$\psi(r_{ij}) = \begin{cases} A_2 \exp[-p_2(\frac{r_{ij}}{r_0} - 1)], & r_{ij} \leq r_{m2} \\ A_{2m} \exp[-p_{2m}(\frac{r_{ij}}{r_0} - 1)](\frac{r_{c2}}{r_0} - \frac{r_{ij}}{r_0})^{n2}, & r_{m2} < r_{ij} \leq r_{c2} \end{cases} \tag{6}$$

where E_i is the total potential energy of an atom i, ϕ and ψ are called here the pair term and density term. r_{m1} and r_{m2} are the knots, and r_{c1} and r_{c2} are the cutoff radii of the pair term and density term, respectively. n_1 and n_2 are the indices which should not be less than 3 and 5, respectively, in order to avoid discontinuity of the high derivatives. A_1, p_1, A_{1m}, and p_{1m} and A_2, p_2, A_{2m}, and p_{2m} are another eight adjustable potential parameters. From Eqs. (5) and (6), one can see that the pair and density terms as well as their high derivatives could continuously and smoothly go to zero at the cutoff radii r_{c1} and r_{c2}, thus removing the 'jumps' of energy and force and avoiding non-physical behaviors in simulations.[10] In order to totally avoid the discontinuity of the energy, pressure and force in the whole calculated range, the pair and density terms as well as their first derivatives should also be continuous at the

transition knots r_{m1} and r_{m1} when fitting the potential parameters. Meanwhile, the cutoff radius r_{c2} is generally set beyond the second neighboring distance at least, in order to distinguish the energy difference between the *fcc* and *hcp* structures.

2. Verification of Simulation Scheme

In the present study, the final energies of the Mg-Cu-Y models are derived by relaxing the constructed solid solution models at 300 K for sufficient simulation time. In addition to the present simulation route, there are several other types of simulation routes as well, for example, by liquid melt quenching, or annealing, to accelerate the sampling of phase-space. To verify the present simulation scheme, we take the alloy of $Mg_{64}Cu_{16}Y_{20}$ as example. The final energies are derived and compared by the following three types of simulation routes: (1) relaxing at 300 K; (2) melting (for example, at 2300 K) and cooling down to 300 K; (3) annealing (for example, at 50 K below *T*g) and cooling to 300 K. The detailed results are presented as follows.

(1) Relaxing at 300K

After constructing the $Mg_{64}Cu_{16}Y_{20}$ solid solution model, we have allowed the models to evolve in MD simulations for about 4×10^6 timesteps, *i.e.*, 20 ns, until the models have reached a relatively stable state, with all the related dynamic variables keeping almost unchanged with the increasing of simulation time. Fig. S1(a) shows the energy evolution during the simulation procedure. Due to the crystalline-to-amorphous transition, the energy is overall decreased. One can see from Fig. S1(a) that the energy of system is converged to ~-2.467eV/atom, at which the variation gradient is on the order of magnitude of -10^{-10}eV/timestep. This can be further demonstrated in Fig. S1(b), which indicates a negligible energy change in the final 4.5×10^5 timesteps.

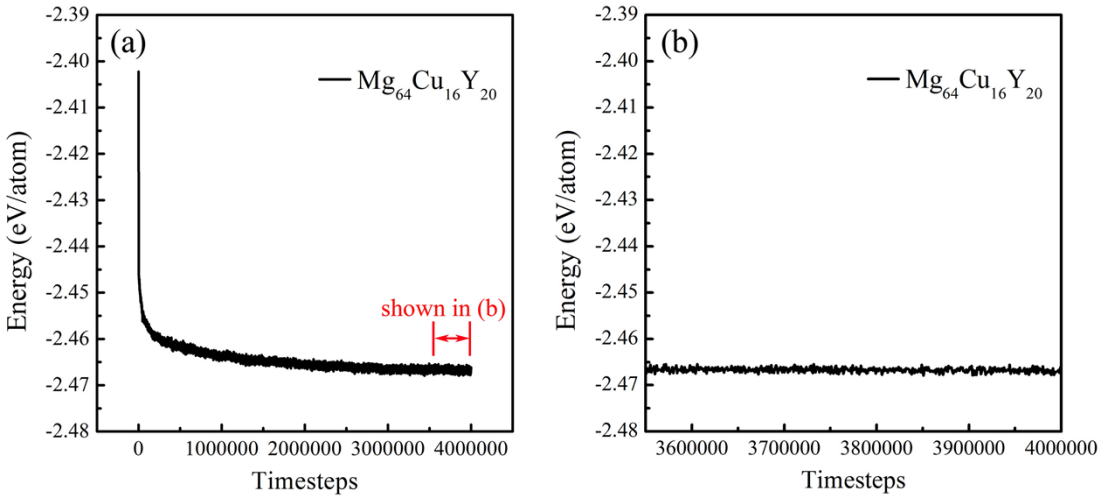

Fig. S1 (a) Evolution of energy per atom during the simulation process for the $Mg_{64}Cu_{16}Y_{20}$ solid solution model. The energy evolution in the final 4.5×10^5 timesteps is specified in (b).

(2) Melting and cooling down to 300K (liquid melt quenching)

In addition to the first simulation route, another common practice to derive the final energy of the system is to simulate the liquid melt quenching process, and the related results are displayed here for comparison. During the simulation process, the system is heated from 300 K to 2300 K at a rate of 5×10^{10} K s^{-1} and equilibrated at 2300 K for 5 ns. The melts are then quenched from 2300 K back to 300 K at the same rate of 5×10^{10} K s^{-1} and equilibrated at 300 K for 5 ns. The heating and cooling rates are set to be quite slow, in order to be close to the experimental condition and provide reasonable reference to the present study. The following Fig. S2 shows the evolution of the system energy for the $Mg_{64}Cu_{16}Y_{20}$ during the quenching process.

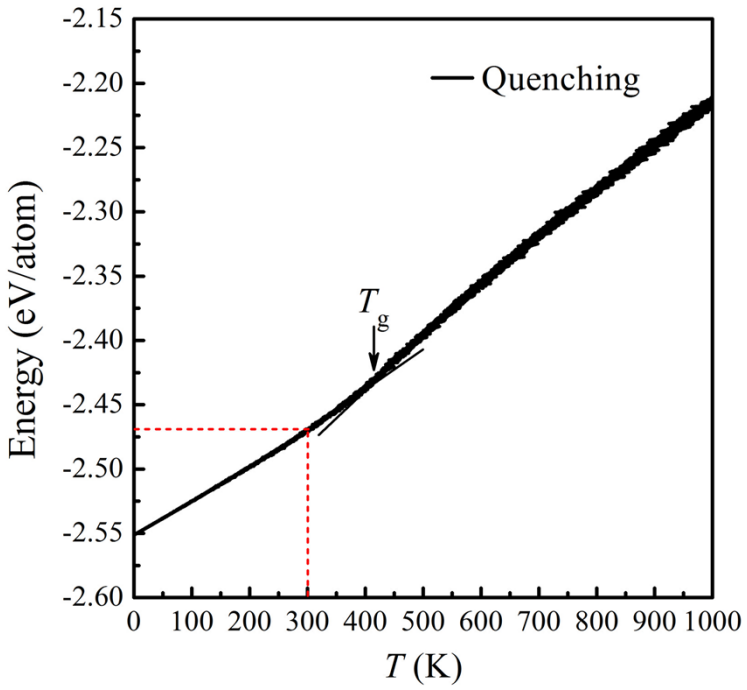

Fig. S2 Evolution of energy per atom as a function of temperature for the $Mg_{64}Cu_{16}Y_{20}$ during quenching process.

From Fig. S2, one can first determine the *T*g of $Mg_{64}Cu_{16}Y_{20}$ to be ~415K. This value is quite close to the experimentally measured *T*g for its adjacent compositions, such as 418 K or 425 K for $Mg_{65}Cu_{25}Y_{10}$,[11] 420 K for $Mg_{65}Cu_{20}Y_{15}$,[12] and 419 K for $Mg_{60}Cu_{30}Y_{10}$,[13] which are all distributed in the regime of 400-450 K. The simulation result is in good accord with the experimental data and lends additional support to our constructed potential. By examining the evolution of energy in Fig. S2, the energy of system at 300K can be determined to be ~-2.469eV/atom. This value is close to the energy derived by relaxing at 300K, *i.e.*, ~-2.467eV/atom, while the minor difference is also negligible in comparison to the magnitude of the calculated formation driving force.

(3) Annealing and cooling to 300K

In order to provide further evidence to the relevance of the simulations, we have considered a third simulation route, *i.e.*, annealing the system obtained by relaxing at 300 K, at a higher temperature, such as at 50K below *T*g, and then cooling the system back to 300 K. Specifically, the system is firstly heated from 300 K to 365 K, *i.e.*, 50K below *T*g, at a rate of 5×10^{10} K s^{-1}, and then annealed at 365 K for 5 ns. Then the system is cooled from 365 K back to 300 K at the same rate of 5×10^{10} K s^{-1}, and then equilibrated at 300 K for 5 ns. The heating and cooling rates are set to be quite slow as well. The following Fig. S3 shows the evolution of system energy during the heating and cooling processes. It can be seen that the annealed energy is also close to that derived by relaxing at 300K, thereby providing further support to the simulation results.

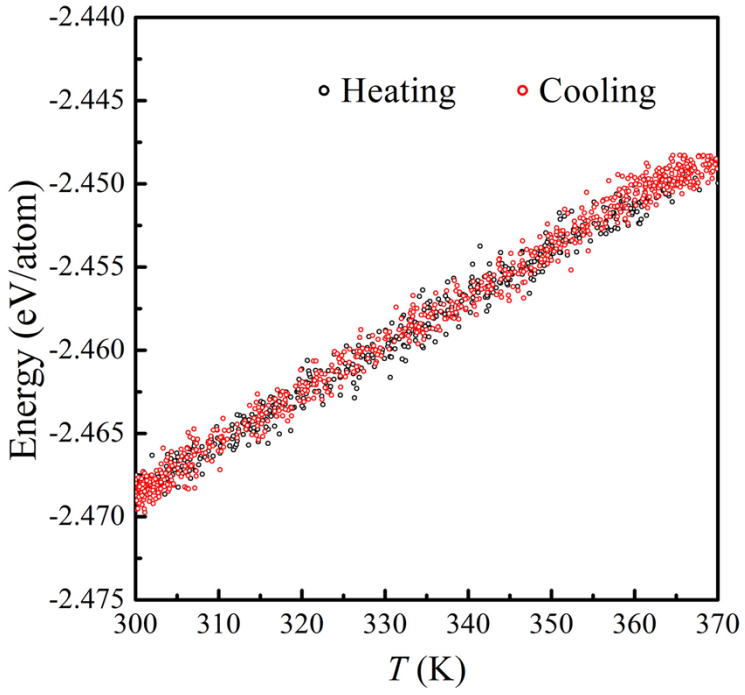

Fig. S3 Evolution of energy per atom as a function of temperature for the $Mg_{64}Cu_{16}Y_{20}$ during the heating and cooling processes.

Summarizing the results by the three simulation routes, it can be concluded that the present simulation route is relevant for Mg-Cu-Y system. In future studies, when extending the present prediction scheme to other systems, especially for the systems with high *T*g, it would be feasible to introduce other types of simulation routes such as annealing to accelerate the sampling of the phase-space.

3. Comparison of Resultant Structure

The atomic configurations of the metallic glasses in the present study are derived by the solid-state crystalline-to-amorphous transition, which is different from the liquid-to-amorphous transition, as involved in the liquid melt quenching process. Therefore, it is of interest to compare the resultant structures derived by the two types of phase transition mechanisms.

For this end, we have selected representative alloys and independently analyzed the atomic configurations derived by the two kinds of phase transformations. It turns out that they exhibit no intrinsic differences in the various structural analyses, such as pair correlation function, Voronoi tessellation and Honeycutt-Anderson analyses. We also take the optimized alloy of $Mg_{64}Cu_{16}Y_{20}$ as example. The atomic configurations and pair correlation functions derived by the two kinds of phase transformation are displayed in Fig. S4. It can be seen that the resultant atomic configurations are statistically equivalent. The simulation procedure of the liquid melt quenching is as introduced in Sec. 2.

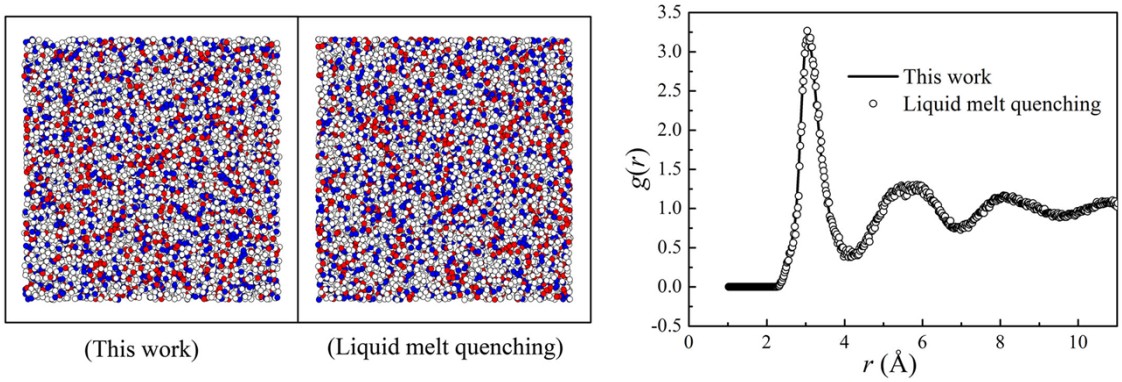

Fig. S4 Comparison of atomic configurations and pair correlation functions derived for the $Mg_{64}Cu_{16}Y_{20}$. Open circle is for Mg, red circle for Cu, and blue circle for Y.

Therefore, it is evidenced that the two categories of transformation can both result in realistic atomic configurations of metallic glasses and provide opportunities to examine the metallic glass formation from different perspectives. The present phase transition route enables one to directly examine the competition and relative stability between the solid solutions and metallic glasses, and also to investigate the underlying physics of phase transition.

References

1 D. Tománek, A. A. Aligia and C. A. Balseiro, *Phys. Rev. B*, 1985, 32, 5051-5056.

2 F. Cleri and V. Rosato, *Phys. Rev. B*, 1993, 48, 22-33.

3 V. Rosato, M. Guillope and B. Legrand, *Philos. Mag. A*, 1989, 59, 321-336.

4 M. W. Finnis and J. E. Sinclair, *Philos. Mag. A*, 1984, 50, 45-55.

5 M. I. Baskes, *Phys. Rev. Lett.*, 1987, 59, 2666-2669.

6 M. I. Baskes, *Phys. Rev. B*, 1992, 46, 2727-2742.

7 B.-J. Lee and M. I. Baskes, *Phys. Rev. B*, 2000, 62, 8564-8567.

8 D. Frenkel and B. Smit, *Understanding molecular simulation: from algorithms to applications*, Academic press, New York, 2001.

9 J. H. Li, X. D. Dai, T. L. Wang and B. X. Liu, *J. Phys.: Condens. Matter*, 2007, 19, 086228.

10 J. H. Li, Y. Dai and X. D. Dai, *Intermetallics.*, 2012, 31, 292-320.

11 W. H. Wang, *J. Appl. Phys.*, 2011, 110, 053521.

12 G. Yuan, T. Zhang and A. Inoue, *Mater. Trans.*, 2003, 44, 2271-2275.

13 S. Linderoth, N. H. Pryds, M. Ohnuma, A. S. Pedersen, M. Eldrup, N. Nishiyama and A. Inoue, *Mater. Sci. Eng. A*, 2001, 304–306, 656-659.